Available online at www.sciencedirect.com
ScienceDirect
Icarus 191 (2007) 702–711
ICARUS
www.elsevier.com/locate/icarus

Arecibo radar observations of Rhea, Dione, Tethys, and Enceladus

G.J. Black [a,*], D.B. Campbell [b], L.M. Carter [c]

[a] *Department of Astronomy, University of Virginia, PO Box 400325, Charlottesville, VA 22904, USA*
[b] *Department of Astronomy, Cornell University, Ithaca, NY 14853, USA*
[c] *Smithsonian Institution, Center for Earth and Planetary Studies, Washington, DC 20013, USA*

Received 19 September 2006; revised 25 May 2007

Available online 25 July 2007

Abstract

We have measured the bulk radar reflectance properties of the mid-size saturnian satellites Rhea, Dione, Tethys, and Enceladus with the Arecibo Observatory's 13 cm wavelength radar system during the 2004 through 2007 oppositions of the Saturn system. Comparing to the better studied icy Galilean satellites, we find that the total reflectivities of Rhea and Tethys are most similar to Ganymede while Dione is most similar to Callisto. Enceladus' reflectivity falls between those of Ganymede and Europa. The mean circular polarization ratios of the saturnian satellites range from ~0.8 to 1.2, and are on average lower than those of the icy Galilean satellites at this wavelength although still larger than expected for single reflections off the surface. The ratio for the trailing hemisphere of Enceladus may be the exception with a value $\simeq$0.56. The 13 cm wavelength radar albedos and polarization ratios may be systematically lower than similar results from the Cassini orbiter's RADAR instrument at 2.2 cm wavelength [Ostro, S.J., and 19 colleagues, 2006. Icarus 183, 479–490]. Overall, these reflectivities and polarization properties, together with the shapes of the echo spectra, suggest subsurface multiple scattering to be the dominant reflection mechanism although operating less efficiently than on the large icy moons of Jupiter. All these saturnian moons and icy jovian moons are atmosphere-less, low temperature water ice surfaces, and any differences in radar properties may be indicative of differences in composition or the effects of various processes that modify the regolith structure. The degree of variation in radar properties with wavelength on each satellite may constrain the thickness and efficiency of the scattering layer.

Keywords: Saturn, satellites; Radar observations; Enceladus

1. Introduction

Saturn's moons Rhea, Dione, Tethys, and Enceladus are a class of airless, icy bodies 500 to 1500 km in diameter that despite these relatively small sizes still show evidence of varying degrees of geologic activity in the past (Plescia and Boyce, 1985) and, in the case of Enceladus, the present (Porco et al., 2006). The collective formation of these moons and subsequent evolution remains an outstanding problem. Their bulk densities range from a high of 1.6 g/cm^3 for Enceladus (Porco et al., 2006) to perhaps as low as 1.0 g/cm^3 for Tethys (Dourneau and Baratchart, 1999), betraying compositions of mostly water ice but with formation histories that led to differing non-ice fractions and interior structure. Compositions are likely related to the positions of their formation from Saturn, especially with regard to the fraction of ammonia (e.g., Mosqueira and Estrada, 2003) which is expected to be prevalent in these satellites due to the cool temperatures in the saturnian nebula (Lewis, 1972). The Cassini mission has recently performed close flybys of these moons, confirming that varying degrees of geologic activity (Wagner et al., 2006) were sustained for an extended period of time on these small objects after their formation, and continuing to the present on Enceladus (Porco et al., 2006). The surfaces of each are known to be fairly clean water ice (Clark et al., 1984) with high optical albedos, and with each exhibiting color and brightness variations indicating heterogeneous coverage of non-ice impurities and surface microstructure. Large scale variations take the form of leading versus trailing hemisphere asymmetries (Buratti and Veverka, 1984), which for these synchronously rotating bodies may be related to interactions with Saturn's magnetospheric plasma and/or the diffuse

* Corresponding author. Fax: +1 434 924 3104.
E-mail address: gblack@virginia.edu (G.J. Black).

0019-1035/$ – see front matter
doi:10.1016/j.icarus.2007.06.009

E-ring in both of which these moons are embedded (Verbiscer et al., 2007), or focusing of micrometeorite impacts due to their orbital motion (cf. Buratti et al., 1990).

Measurements of radar properties and any inter-satellite variations can address these issues of surface characteristics and formation histories. The radar reflectivity of a surface depends on its composition and structure, so we undertook an effort to measure the radar scattering properties of these objects. Materials with high dielectric constants and loss tangents, such as the silicate surfaces of the terrestrial planets and asteroids, will to first order yield reflections from the vacuum-surface interface and have radar albedos of $\lesssim$0.2 (cf. Ostro, 1993). For surfaces smooth on horizontal scales within roughly an order of magnitude of the incident wavelength, single reflections dominate and the reflectivity is directly related to the bulk dielectric constant of the surface. In contrast, surfaces of water ice, if extremely clean and at temperatures around 100 K, can have essentially negligible absorption at radio wavelengths (cf. Thompson and Squyres, 1990) and subsurface multiple scattering mechanisms become important. Thus the radar can probe wavelength-scale structures not only on, but below the surface at depths which depend (perhaps sensitively) on non-ice contaminants. The canonical examples of this property are the icy Galilean satellites for which there is no evidence of specular surface reflections at wavelengths from 3.5 up to 70 cm, and their entire echoes are apparently the result of multiple scattering (Campbell et al., 1978; Ostro et al., 1992; Black et al., 2001a). They are strongly backscattering and preferentially preserve the polarization sense under circularly polarized illumination, a signature of multiple scattering and unlike single reflections which reverse the sense.

Various models have been explored to quantitatively explain the high albedos and polarization ratios. All rely on subsurface scattering and range from those that consider the effects of buried structures such as craters (Baron et al., 2003; Gurrola, 1995; Eshleman, 1986), randomly oriented facets (Goldstein and Green, 1980), or refractive lenses (Hagfors et al., 1997), to models of distributions of non-specific but efficient scatterers (Black et al., 2001b) that produce a coherent enhancement in the backscatter direction (cf. Hapke, 1990; Peters, 1992). We present new 13 cm wavelength radar observations of mid-size saturnian satellites and only a few qualitative interpretations, leaving quantitative modeling for future efforts.

2. Observations

We observed these saturnian satellites with the Arecibo Observatory's 13 cm (2.4 GHz) radar system during four epochs from 2004 through early 2007 at times near opposition in order to minimize the Earth-to-target distances. A log of the observations is given in Table 1. The round-trip light-travel time to the Saturn system at opposition is ~2.25 h, permitting ~30 min of observing time per day due to the Arecibo telescope's restricted elevation range. Equipment problems resulted in some observing sessions being shorter than this maximum tracking time. In 2006 only half the transmitted power relative to prior years was available since one of the two transmitter klystrons was out for maintenance.

In 2004, short radar observations of the icy Galilean satellites whose radar characteristics are well known were made to assist in calibrating the telescope gain, which is 73.3 db averaged over the zenith angles of 12.5°–19.7° covered by the observations, consistent with routinely measured standard astronomical calibrators. For the Arecibo telescope, both gain and system temperature are functions of zenith position. The system temperature was measured nightly and varied between 25 and 32 K. Depending on its location in the beam, the thermal flux from Saturn can increase the base system temperature by about 10%, as expected from its decimeter brightness temperature of ~200 K (de Pater and Dickel, 1991). Reflection of the radar signal from the ring system is also received, but is spread over ~650 kHz and blends into the spectral background removed during reduction. With the reflectivity of the rings around 30–40% (Nicholson et al., 2005), they contribute at most 0.5 K to the system temperatures.

On each date a circularly polarized monochromatic signal was transmitted and the echo was recorded in both circular polarizations, labeled as SC for the same circular sense as the transmitted signal and OC for the opposite circular sense. Spectra of the recorded signals were then made to isolate the echo in frequency. The rotation of a satellite induces a varying Doppler shift in the reflected signal across its disk. For these targets this effect spreads their echos into bandwidths of order several 100s of Hz at the radar's frequency. Table 2 gives the physical parameters of each satellite and the resulting average Doppler bandwidth of each, which varies by $\sim \pm 3\%$ year-to-year due to the changing latitude of the sub-Earth track. Only this average bandwidth was used in the final analysis. For each target, the spectra, s_i, from all dates are weighted and summed to produce a final echo spectrum, S, as shown in Fig. 1 according to

$$S = \frac{\sum w_i s_i}{\sqrt{\sum w_i^2}}, \tag{1}$$

where the weight for each spectrum is given by

$$w_i = \frac{P g_t g_r \sqrt{\tau}}{T_{\mathrm{sys}}}, \tag{2}$$

for transmitted power P, antenna gains g_t and g_r at transmit and receive positions respectively, integration time τ, and system temperature T_{sys}. Disk integrated scattering parameters reduced from these spectra are given in Table 3. The total echo power in each spectrum was converted to a physical cross section via the system parameters and known target distance, then normalized by the target's projected area to convert into a specific cross section, hereafter referred to as the radar albedo.

Unless noted, the quoted uncertainties used here represent one standard deviation of the noise statistics and not possible systematic errors, which could be as much as 25% if errors in the transmitted power, system temperature, and telescope gain are all of order 10%. Such systematic errors should affect all results equally and the circular polarization ratio, which is defined to be the ratio of the power in the SC channel to that

Table 1
Observation log

Target	Date (UT)	W. longitude (deg)	W. latitude (deg)	Beam separation[a] (arcmin)	Obs. time (min)	Power (kW)
Enceladus	2004 Jan 17	92	−28	0.39	30	740
	2005 Jan 23	260	−25	–	30	801
	2005 Jan 24	161	−25	0.45	27	795
	2005 Jan 31	196	−25	–	29	771
	2005 Feb 01	98	−25	–	29	802
	2005 Feb 03	262	−25	0.17	25	779
	2006 Feb 08	265	−21	–	30	439
	2006 Feb 09	167	−21	–	29	444
	2007 Jan 24	68	−15	–	22	649
	2007 Jan 26	232	−15	–	25	649
	2007 Jan 27	134	−15	–	25	642
	2007 Jan 28	36	−15	0.33	29	741
	2007 Feb 04	71	−15	0.58	26	655
	2007 Feb 05	333	−15	0.58	26	756
	2007 Feb 07	135	−15	–	26	800
	2007 Feb 08	39	−15	–	26	877
Tethys	2005 Jan 23	299	−23	0.21	30	801
	2005 Jan 24	130	−23	–	27	795
	2005 Jan 25	320	−23	–	18	782
	2005 Feb 02	41	−23	–	17	790
	2005 Feb 03	232	−23	–	25	779
	2006 Feb 08	221	−19	0.24	30	439
	2006 Feb 09	51	−19	0.59	29	444
	2006 Feb 11	72	−19	0.29	29	442
	2007 Jan 24	6	−15	0.57	22	649
	2007 Jan 28	47	−15	0.72	29	741
	2007 Feb 07	149	−15	0.07	26	800
	2007 Feb 08	339	−15	0.73	26	877
Dione	2004 Jan 17	36	−26	–	29	740
	2005 Jan 24	125	−23	0.22	27	795
	2005 Jan 31	324	−23	0.75	29	771
	2005 Feb 01	95	−23	0.40	29	802
	2006 Feb 09	186	−19	0.29	29	444
	2006 Feb 11	88	−19	–	29	442
	2007 Jan 24	7	−13	0.50	22	649
	2007 Jan 26	270	−13	0.54	25	649
	2007 Jan 27	41	−13	0.36	25	642
	2007 Jan 28	172	−13	0.75	29	741
	2007 Feb 07	44	−14	0.40	26	800
	2007 Feb 08	176	−14	0.51	26	877
Rhea	2004 Jan 16	318	−26	–	29	720
	2004 Jan 17	37	−26	0.27	22	740
	2004 Jan 18	117	−26	–	29	767
	2005 Jan 25	307	−23	0.68	18	782
	2005 Feb 03	303	−23	0.81	25	779
	2006 Feb 08	256	−19	0.75	30	439
	2006 Feb 11	134	−19	0.33	29	442
	2007 Jan 24	58	−13	0.61	22	649
	2007 Jan 26	218	−13	0.37	25	649
	2007 Jan 28	17	−13	0.15	29	741
	2007 Feb 08	171	−13	0.48	26	877

[a] No entry indicates the primary target on that date and thus centered in the beam. Titan was the primary target on 2007 Jan 28, Feb 4, Feb 5.

in the OC channel, should be largely immune to systematic errors in the gain and transmitter power in particular. Consistent 13 cm wavelength radar measurements of inner Solar System targets and the icy Galilean satellites over more than three decades have demonstrated the stability of the system calibration within the statistical uncertainties of those measurements. We further note the system stability shown by the results of multi-epoch observations of the stronger Saturn system targets Titan (Campbell et al., 2003) and the ring system (Nicholson et al., 2005). Thus systematic errors and absolute calibration issues should be significant only when comparing Arecibo observations with those of other systems at other wavelengths,

Table 2
Satellite parameters

Target	Diameter (km)	Rotation (h)	Bandwidth (Hz)
Rhea	1529	108.43	368
Dione	1123	65.69	451
Tethys	1066	45.31	615
Enceladus	504	32.88	400

The bandwidth is the frequency spread of the echo due to the target's rotation and is given by $B = 4\pi D \cos\delta/\lambda P$ for diameter D, rotation period P, wavelength λ (=13 cm), and subradar latitude δ. These bandwidths are averages over the different latitudes in Table 1. Diameters are from Thomas et al. (2006).

such as from the Cassini RADAR at 2.2 cm wavelength as discussed later.

Since the angular separation between satellites if often less than the width of the Arecibo beam at this wavelength, on many dates more than one satellite could be observed simultaneously. At those times one satellite was selected as the primary target and centered in the beam with the secondary target(s) falling at some angular distance off-center as indicated in Table 1. The beam shape was assumed to be Gaussian with an average half power beam width of 1.95 arcmin (Heiles et al., 2000) and included by modifying the gains in the weighting function. Secondary targets would also drift in frequency due to their motion relative to the primary by as much as ~10 Hz/s, which was corrected by frequency drifting the raw sampled data

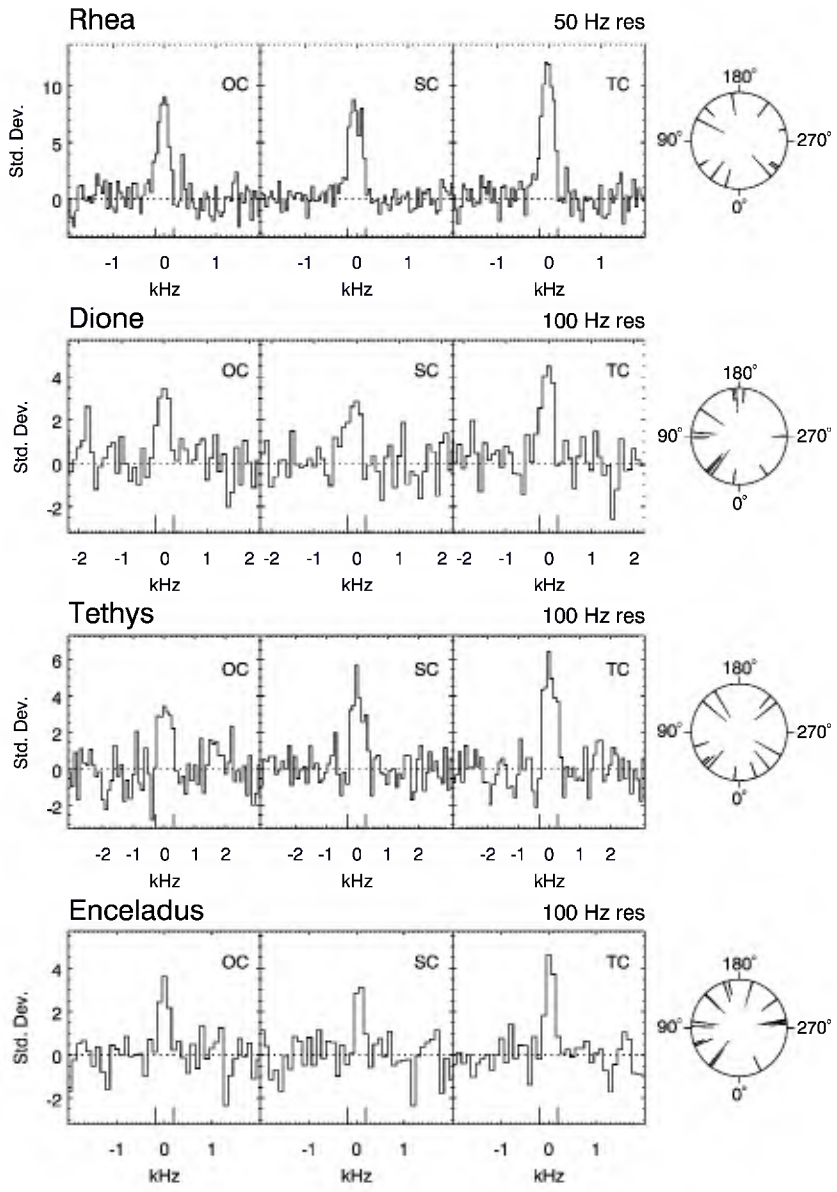

Fig. 1. Final summed 13 cm wavelength echo spectra are shown for each target. Panels show the power received in the opposite circular sense as transmitted (OC), same circular sense (SC), and their weighted sum (TC). Short bars on the abscissas indicate the average expected bandwidth of each target due to the rotationally induced Doppler shifts of the signal (see Table 2). The frequency resolution used in each row is indicated; a smaller resolution is used for Rhea given its higher signal-to-noise ratio (SNR). The ordinate scales are standard deviations of the noise. The inward pointing lines in the last panel indicate the central west longitudes of each observation on that target, with the length of the line proportion to the weight function for each.

Table 3
Satellites' 13 cm wavelength radar properties

Target		Radar albedo	μ_C (SC/OC)	SNR	B_{eq}/B
Rhea	OC	0.61 ± 0.03		46	0.90 ± 0.03
	SC	0.71 ± 0.04		49	0.97 ± 0.02
	TC	1.31 ± 0.05	1.17 ± 0.09		
Dione	OC	0.41 ± 0.07		11	0.93 ± 0.09
	SC	0.32 ± 0.07		8	0.73 ± 0.18
	TC	0.74 ± 0.10	0.81 ± 0.21		
Tethys	OC	0.66 ± 0.09		17	0.97 ± 0.03
	SC	0.79 ± 0.09		20	0.84 ± 0.08
	TC	1.45 ± 0.13	1.22 ± 0.21		
Enceladus (total)	OC	1.07 ± 0.22		8	0.78 ± 0.17
	SC	0.86 ± 0.20		6	0.58 ± 0.22
	TC	1.94 ± 0.31	0.83 ± 0.25		
Enceladus (lead)	OC	1.16 ± 0.29		7	0.79 ± 0.20
	SC	1.39 ± 0.29		8	0.83 ± 0.15
	TC	2.55 ± 0.42	1.28 ± 0.41		
Enceladus (trail)	OC	1.00 ± 0.28		5	0.52 ± 0.28
	SC	$\leqslant$0.54[a]		–	–
	TC	0.78 ± 0.28	$\leqslant$0.56[a]		

Error estimates are based on one standard deviation of the statistical uncertainties.
[a] Three standard deviation upper limit.

during processing prior to forming the power spectra. The absolute frequency difference between targets could be as large as ~100 kHz. Initially a standard frequency hopping technique (cf. Ostro et al., 1992) was used in 2004 where the transmitter frequency alternates at 10 s intervals between four frequencies separated by 10 kHz. This scheme is employed to provide signal-free background samples at the three frequencies not currently used during any given hop period. This was found to be an extra complication when extracting multiple targets and so subsequent sessions used a single transmit frequency. The background at the target's frequency was then obtained by interpolating the smoothly varying bandpass across the echo's narrow bandwidth.

3. Discussion

The final spectra shown in Fig. 1 demonstrate the detection quality of each targeted moon. Generally their radar albedos are high with roughly comparable power returned in both circular polarizations, as listed in Table 3. Such properties strongly indicate a subsurface multiple scattering mechanism, also known as volume scattering, but perhaps operating to somewhat different extents on each moon. Single scattering from the surface would return the majority of power in the OC channel. Single scattering dominates echoes from inner Solar System targets; for example, the Moon at 13 cm wavelength has a total albedo of ~0.07 and a polarization ratio of only ~0.1 (Evans and Hagfors, 1966), and what little power is returned in the SC polarization sense is due to wavelength scale surface and near-surface roughness. Some asteroids reflect comparable power in both polarizations with little specular reflection, however their total albedos remain low (e.g., Magri et al., 1999; Benner et al., 1997), a combination which is usually interpreted to result from considerable surface and near surface wavelength scale roughness. To return significant power in the SC channel would require a more efficient multiple scattering mechanism.

The shape of the echo spectrum gives an indication of the scattering mechanism. If single surface scattering dominates, the echo from a spherical body will be strongest at the sub-radar point where the incidence angle is near vertical producing a strong specular reflection in the center of the echo spectrum. Multiple scattering mechanisms can broaden the spectrum by returning significant power at higher incident angles. This distribution of power within the echo spectrum can be expressed as an equivalent bandwidth, defined in the sense used in Ostro et al. (1992),

$$B_{eq} = \Delta f \frac{[\sum y_i]^2}{\sum y_i^2}, \tag{3}$$

where y_i are the spectrum amplitudes and Δf is the frequency resolution. The broad widths (see Table 3) of the echoes further indicate a multiple scattering mechanism.

The mid-size satellites of Saturn are generically similar to the icy Galilean satellites of Jupiter in that all have low-temperature, water ice dominated surfaces exposed to the vacuum. Thus one might expect the regolith structure of these saturnian moons to be similar to that of the icy Galilean satellites given the dominance of water ice, not too dissimilar cratering rates (Zahnle et al., 2003), and ancient surfaces. The latter point may not hold for Enceladus however in light of recent Cassini observations of current surface activity near its south pole (e.g., Porco et al., 2006), but most of these moons' surfaces have estimated ages of order 2 to 3 Gyr (Plescia and Boyce, 1985). The extremely low absorption of centimeter wavelength radia-

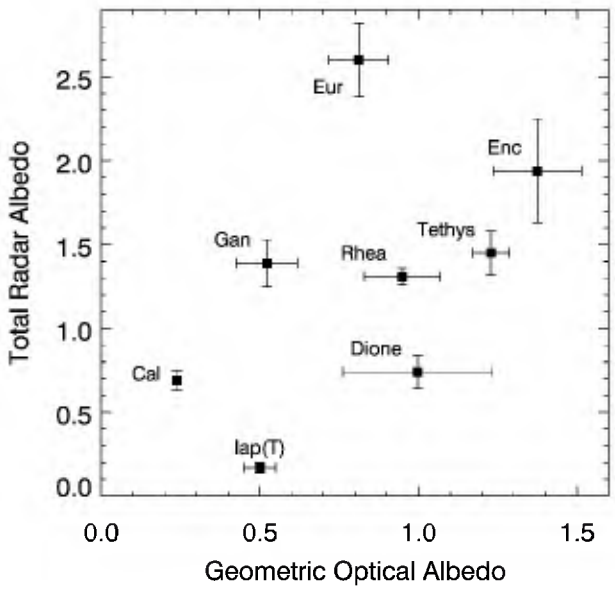

Fig. 2. Comparison of icy satellite 13 cm wavelength radar albedos versus their visual wavelength geometric albedos. For both systems the rough correlation between optical and radar albedos suggests a commonality between the primary darkening agent in both wavelength regimes. Radar error bars represent one standard deviation of the statistical uncertainties, optical error bars represent the range of variation with longitude. Jupiter satellite radar albedos are from Ostro et al. (1992); Iapetus radar albedo from Black et al. (2004). Optical albedos for the Saturn system are from Verbiscer et al. (2007); for the Jupiter system from Domingue and Verbiscer (1997).

tion in clean water ice will permit penetration of the radiation to much greater depths than on non-ice targets. Regolith development will cause density and hence refractive discontinuities, creating a population of scattering centers within these low-loss layers. When observed with a radar, these characteristics of the icy Galilean satellites lead to a condition where they become very effective backscatterers. At 13 cm wavelength Europa's total radar albedo is ~2.6 and its circular polarization ratio 1.5 (Ostro et al., 1992), compared to non-icy, inner Solar System targets which have radar albedos and polarizations ratios an order of magnitude lower. Furthermore, for the icy Galilean satellites the lack of any specular echoes is also consistent with a volume scattering mechanism. If the saturnian satellites have similar regolith properties then their radar albedos and polarization ratios should also be large. Non-Galilean satellite scattering properties would indicate a different surface structure and/or composition, having implications for the current and past conditions in the Saturn system in either case.

The total 13 cm wavelength radar albedos are plotted versus optical geometric albedos in Fig. 2, along with the corresponding values for the icy Galilean satellites. For Europa, Ganymede, and Callisto, there is a good correlation between these two quantities, implying a certain amount of homogeneity between the optical surface and the depths probed by the radar, i.e., several tens of wavelengths. The inter-satellite trend follows the overall icy purity inferred for these moons from their optical albedos and depths of infrared water bands, with Europa having the lowest fraction of non-ice contaminants, Callisto the highest, and Ganymede intermediate (cf. review by Clark et al., 1986). The Saturn satellites have optical albedos similar to the jovian satellites as well as similar water ice band depths in the infrared (Clark et al., 1984), but follow a different trendline in Fig. 2. Thus the general correlation between optical and radar albedos for both satellite systems can be explained with a varying fraction of an optical and radar darkening compound, such as meteoritic material. The shift in the trend for the saturnian satellites suggests their surfaces have an additional radar absorber that reduces contributions from volume scattering but without affecting the optical albedos, thereby depressing the radar reflectivity for a given optical reflectivity. Alternatively, a thin mantling of clean, optically bright ice could increase the optical reflectivity without affecting the radar reflectivity. A coating of small, fresh grains may easily explain Enceladus' properties, but it may be more difficult to cover the other satellites at the optical wavelength scale by such small grains without giving them all Enceladus-like optical properties.

Several classes of compounds can affect the radar scattering by increasing the absorption in a water ice layer. Silicates, organics, or ammonia are plausibly present in the surfaces of these objects. While these new data themselves do not strongly distinguish between possible absorbers, ammonia compounds are likely candidates based on availability, formation models, and comparison to other data obtained at other wavelengths. Ammonia is expected to be more prevalent in the satellites of Saturn than in those of the Jupiter system due to the cooler temperatures in the saturnian nebula (Lewis, 1972), and has been invoked to explain the origin of Titan's nitrogen atmosphere via destruction of its originally accreted ammonia (Atreya et al., 1978; Owen, 2000). In addition, the presence of large quantities of ammonia in the moons' water ice mantles would significantly lower the melting points and maintain liquid or ductile interiors at lower temperatures than is possible in a completely water ice body. Lowering of the melting point in these objects is one means of explaining the evidence of more active geology than would otherwise be expected on these small, cold objects (Squyres et al., 1983). Ammonia in the near-surface should affect the radar reflectivity since it can increase the absorption of centimeter-wavelength radiation considerably (Lorenz and Shandera, 2001) and be less optically active than silicates or organics. To date there has been no robust detection of any significant quantity of ammonia on these objects. Infrared spectra are dominated by strong water features, with other compounds detected or constrained to be present only in trace amounts. For Enceladus, Emery et al. (2005) report a possible detection of ammonia at the level of 0.5% by weight, while Cassini measurements place an upper limit of 2% on its global abundance (Brown et al., 2006). Even the plumes from Enceladus' south polar terrain are at least 90% H_2O with only trace quantities of ammonia (Waite et al., 2006).

Fig. 3 plots the multi-wavelength radar properties of the four icy saturnian satellites discussed here together with those of the trailing hemisphere of Iapetus (Black et al., 2004; Ostro et al., 2006) and the icy Galilean satellites (Ostro et al., 1992; Black et al., 2001a) for comparison. Any comparisons drawn from Fig. 3 depend on the absolute calibration of the different

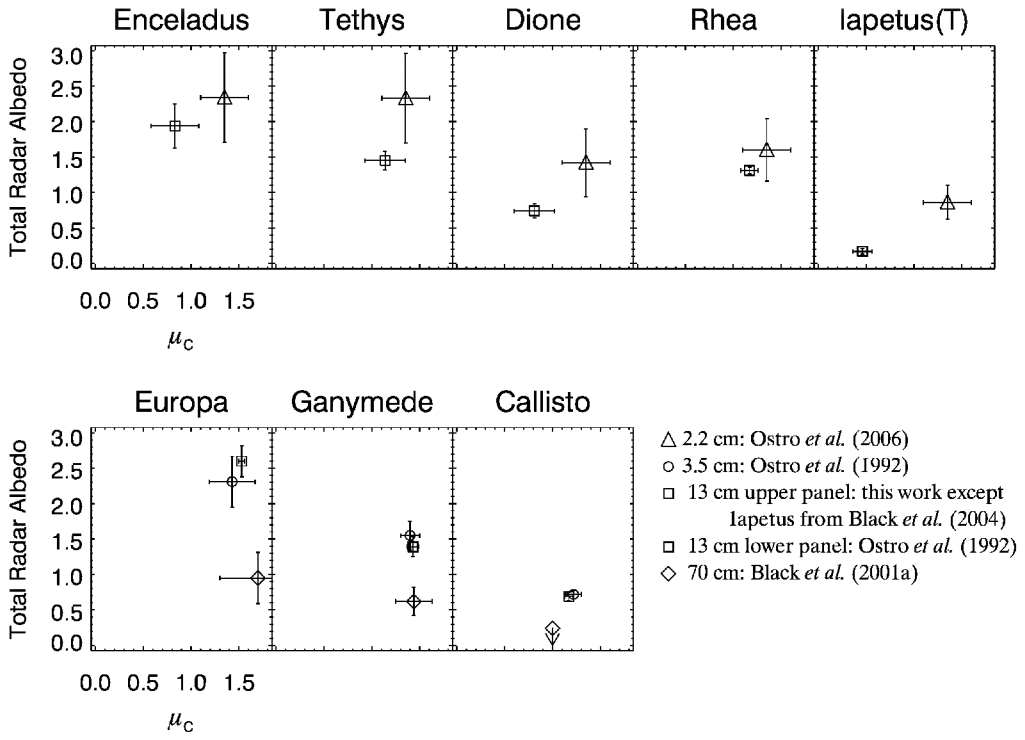

Fig. 3. Plots of total radar albedo versus circular polarization ratio for each target. Panels with data for Iapetus' trailing (icy) hemisphere and for the icy Galilean satellites are included for comparison. Each point includes data from all available longitudes except Iapetus. The abscissa of each panel is the same as the first panel's. Saturn satellite data at 13 cm wavelength are plotted with the quadrature sum of statistical uncertainties and a 25% systematic uncertainty. At 2.2 cm wavelength the error bars further include assumptions in the ranges of polarization ratios (see text and Ostro et al., 2006). Error bars for the Galilean satellites are the larger of the statistical uncertainties or the range of any variation with longitude.

instruments, and so for these new data the radar albedo error bars in that figure represent the quadrature sum of the statistical uncertainties and a 25% systematic error. Furthermore, while we have directly measured the radar properties in both circular polarizations at 13 cm wavelength, the values at 2.2 cm wavelength from Cassini were obtained in a single linear polarization only. For those measurements, Ostro et al. (2006) assumed polarization behavior similar to that of the icy Galilean satellites in order to convert the single linear polarization into a total radar albedo. Barring other information, this appears to be justified given the already high albedos observed in that one linear polarization alone. Finally, the total radar albedo would then be the same whether measured in linear or circular polarization. For the Cassini points in Fig. 3 we have incorporated the same assumptions for linear and circular polarizations from Ostro et al. (2006) into the error bars on the Cassini measurements, namely that the linear polarization ratio is in the range [0.0, 0.7] and the circular polarization ratio is in the range [1.1, 1.6]. That latter range is inconsistent with these 13 cm observations, but taking the circular polarization ratios at 2.2 cm wavelength to be equal to those 13 cm wavelength, as observed for the Galilean satellites, does not align the radar albedos at those two wavelengths in Fig. 3. There also does not seem to be any single systematic correction factor as would result from an absolute calibration difference that better aligns the two radar datasets for all saturnian satellites.

The new measurements presented here overall show lower total albedos and lower polarization ratios than those of the icy Galilean satellites, and, keeping in mind the assumptions in the previous paragraph, may show a greater disparity between wavelengths for the saturnian targets. The icy Galilean satellites show nearly identical properties at both 13 and 4 cm wavelength scales, with significant reduction in radar albedo evident only at the much longer wavelength of 70 cm. The saturnian satellites observed here, as well as Iapetus, instead may show real differences between the shorter two wavelengths.

While the apparent drops in saturnian satellites radar albedos between 2.2 and 13 cm wavelengths somewhat mirrors the drops between 13 and 70 cm wavelengths on the icy Galilean satellites, the polarization ratios may also drop for the former set. The icy Galilean satellites' albedo drop from 13 to 70 cm wavelength has been interpreted as a reduction in the number of scatterers at the larger wavelength (Black et al., 2001b). The drop between wavelengths observed on Iapetus was suggested by Ostro et al. (2006) to result from a relatively shallow scattering layer. These new data may further support their suggestion that the effective scattering layers on these moons are determined by an increasing amount of absorber with depth, such that relatively cleaner layers are seen by the 2.2 cm wavelength, while the 13 cm wavelength senses lower, more absorbing layers.

Any drop in polarization ratio from 2.2 to 13 cm wavelength would likewise be due to increasing absorption reducing the efficiency of volume scattering as longer scattering paths that preserve the incident polarization sense are the paths that suffer relatively more attenuation. The result of any added absorption

at 13 cm wavelength is thus to reduce both the radar albedo and the polarization ratio. Conversely, the polarization ratios of the icy Galilean satellites may remain high at all wavelengths because their albedo drop with wavelength is due instead to a lack of scatterers available at the largest scales (Black et al., 2001b), effectively diminishing the number of scattering paths without preferentially selecting against longer ones.

3.1. Rhea

These results confirm the preliminary analysis of a subset of these Rhea data by Black and Campbell (2004). In terms of radar properties, Rhea is a close analogue to Ganymede at both the 13 cm wavelength and the 2.2 cm Cassini wavelength. With a closer optical albedo match to Europa, this suggests that the radar senses a Ganymede-like subsurface but with an optically bright coating thin on the radar wavelength scale. Also like Ganymede, there is little difference between Rhea's properties at both radar wavelengths, implying that the surface appears similar on both wavelength scales. Such a homogeneity may be consistent with Rhea having the oldest and thus most well-mixed regolith as inferred from cratering statistics (Plescia and Boyce, 1985).

We have also split the data set into leading ($0° \leqslant$ west longitude $< 180°$) and trailing ($180° \leqslant$ west longitude $< 360°$) hemispheres. The Cassini RADAR observed only the leading hemisphere of Rhea (Ostro et al., 2006). The ratios of the hemispherically separate 13 cm wavelength radar albedos versus the similar ratio of hemispheric optical albedos are plotted in Fig. 4. The leading side is significantly more reflective than the trailing side at both optical (Verbiscer et al., 2007) and 13 cm radar wavelengths, indicating that perhaps the same material or process darkens the surface in both wavelength regimes.

3.2. Tethys

Tethys has 13 cm wavelength radar properties very similar to Rhea and Ganymede, but possibly different values than at the Cassini 2.2 cm wavelength. A decrease in albedo and polarization ratio may signal a decrease in volume scattering via an increased absorption seen at depth by the longer wavelength. If real, this difference may constrain a gradient in composition or structure with depth.

The breakdown of the Tethys dataset into leading and trailing hemispheres is also shown in Fig. 4. No significant asymmetry in radar albedo is seen. The Cassini RADAR observed only the trailing hemisphere of Tethys (Ostro et al., 2006).

3.3. Dione

Dione's albedos at both radar wavelengths are lower than the corresponding values for Tethys and with possibly a larger wavelength dependence. One way to achieve this is for Dione's surface layers to contain a higher fraction of radar absorbing material, lowering the overall radar albedo and decreasing the effectiveness of any volume scattering. A decrease in the relative contribution of volume scattering over single surface scattering would have the effect of lowering the polarization ratio as seems to be the case at 13 cm wavelength. At 2.2 cm wavelength Dione's radar albedo is similar to Rhea's, but if Dione's albedo drops by 13 cm wavelength it may suggest a steeper gradient in composition or structure with depth than Rhea, causing a quicker decrease in volume scattering efficiency at 13 cm wavelength on Dione.

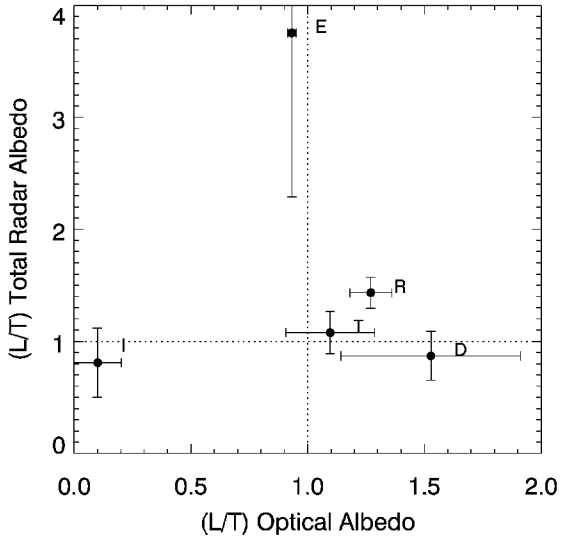

Fig. 4. Comparison between the ratios of leading to trailing hemisphere albedos at 13 cm radar wavelength (this work) versus at optical wavelengths (Verbiscer et al., 2007). The radar albedo points are shown with statistical uncertainties as systematic errors should factor out in the ratio. Rhea and Enceladus appear to have significantly higher radar albedos on their leading sides, in phase with the optical asymmetry for Rhea and out of phase for Enceladus. Dione and Iapetus show no significant hemispheric difference in 13 cm wavelength radar albedo despite large optical asymmetries.

Like Tethys, there does not appear to be a significant difference in radar properties between leading and trailing hemispheres within the statistical uncertainties, despite its quite large optical asymmetry (Verbiscer et al., 2007). Our observations are much more concentrated on Dione's leading side and very sparse on it's trailing side however. Only the leading hemisphere of Dione has been observed by the Cassini RADAR (Ostro et al., 2006).

3.4. Enceladus

Enceladus' total radar albedo is the highest of these moons, although its 13 cm wavelength polarization ratio is relatively low. The effective backscattering needed for a high albedo cannot rely on single scattering, and hence the required multiple scattering should also result in a similarly very high polarization ratio. The radar albedos at both radar wavelengths appear essentially identical, although the polarization ratios may not be. If real, these results may be more difficult to explain than the wavelength variations seen on the other satellites. Unfortunately the Enceladus detection does not have the high signal-to-noise ratio one would like to robustly draw further conclusions.

As shown in Figs. 4 and 5, splitting the Enceladus data into leading and trailing hemispheres indicates that most of the received radar signal apparently comes from the leading hemi-

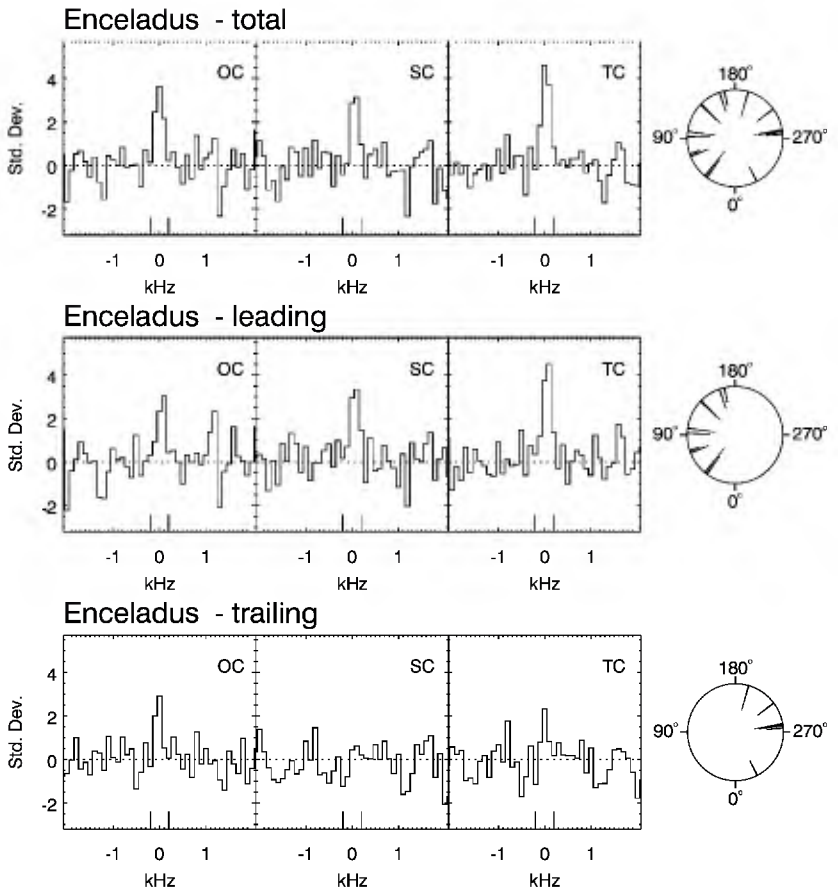

Fig. 5. Enceladus 13 cm wavelength echo spectra split into leading and trailing hemisphere data sets. The top panel reproduces Fig. 1 and contains data from all longitudes. See Fig. 1 for description of axes and clock diagrams. Most of the Enceladus echo appears to originate from the leading hemisphere. There is no detection of the trailing hemisphere in the SC polarization, suggesting a very low polarization ratio for an icy surface. The overall sensitivity on the leading side is only about 15% better than on the trailing side due mainly to the larger number of observing sessions on the former.

sphere, indicating a substantial radar asymmetry. These hemispherically separate results are also included in Table 3. Compared to the slight optical hemispheric asymmetry (Verbiscer et al., 2007), the radar asymmetry supports the model of Enceladus having a thin mantling of fresh, clean ice particles that is transparent to the radar which instead senses deeper, older, and perhaps a more original surface. The lack of a detection of the trailing hemisphere in the SC polarization channel suggests a surprisingly low polarization ratio for an icy surface. As a result of the geometry, latitudes southward of ~70° S were in continuous view during our observations, including most of the south polar terrain (Porco et al., 2006), which cannot then be used to explain a hemispheric difference seen here.

If other processes besides impact gardening have been recently modifying Enceladus' surface, its structure may be dramatically different than the older, mature regolith of the other satellites. A combination of high radar albedo and low polarization ratio may indicate unique surface properties. On the Earth, the melt zones of the Greenland ice sheet have this combination of radar properties, apparently due to subsurface ice structures that result from seasonal melting and refreezing cycles (Rignot et al., 1993; Jezek et al., 1994), as do some high altitude glaciers in the Andes and Tibet (Haldemann and Muhleman, 1999). Although liquid water content controls the radar reflectivity of Earth's ice surfaces, those studies generically suggest that the radar scattering from Enceladus may be controlled by structures not found on the other icy satellites.

Acknowledgments

G.J.B. acknowledges support from the NASA Planetary Astronomy Program and D.B.C. acknowledges support from the NASA Planetary Geology and Geophysics Program. The Arecibo Observatory is part of the National Astronomy and Ionosphere Center, which is operated by Cornell University under a cooperative agreement with the National Science Foundation.

References

Atreya, S.K., Donahue, T.M., Kuhn, W.R., 1978. Evolution of a nitrogen atmosphere on Titan. Science 201, 611–613.

Baron, J.E., Tyler, G.L., Simpson, R.A., 2003. Three-dimensional numerical modeling of refraction and reflection scattering from icy Galilean satellites. Icarus 164, 404–417.

Benner, L.A.M., and 12 colleagues, 1997. Radar detection of near-Earth Asteroids 2062 Aten, 2101 Adonis, 3103 Eger, 4544 Xanthus, and 1992 QN. Icarus 130, 296–312.

Black, G., Campbell, D., 2004. Rhea's surface: Ice properties measured by radar. Bull. Am. Astron. Soc. 36. Abstract 1123.

Black, G.J., Campbell, D.B., Nicholson, P.D., 2001b. Icy Galilean satellites: Modeling radar reflectivities as a coherent backscatter effect. Icarus 151, 167–180.

Black, G.J., Campbell, D.B., Ostro, S.J., 2001a. Icy Galilean satellites: 70 cm radar results from Arecibo. Icarus 151, 160–166.

Black, G.J., Campbell, D.B., Carter, L.M., Ostro, S.J., 2004. Radar detection of Iapetus. Science 304, 553.

Brown, R.H., and 24 colleagues, 2006. Composition and physical properties of Enceladus' surface. Science 311, 1425–1428.

Buratti, B., Veverka, J., 1984. Voyager photometry of Rhea, Dione, Tethys, Enceladus and Mimas. Icarus 58, 254–264.

Buratti, B.J., Mosher, J.A., Johnson, T.V., 1990. Albedo and color maps of the saturnian satellites. Icarus 87, 339–357.

Campbell, D.B., Chandler, J.F., Ostro, S.J., Pettengill, G.H., Shapiro, I.I., 1978. Galilean satellites—1976 radar results. Icarus 34, 254–267.

Campbell, D.B., Black, G.J., Carter, L.M., Ostro, S.J., 2003. Radar evidence for liquid surfaces on Titan. Science 302, 431–434.

Clark, R.N., Fanale, F.P., Gaffey, M.J., 1986. Surface composition of natural satellites. In: IAU Colloq. 77: Some Background about Satellites, pp. 437–491.

Clark, R.N., Steele, A., Brown, R.H., Owensby, P.D., 1984. Saturn's satellites—Near-infrared spectrophotometry (0.65–2.5 microns) of the leading and trailing sides and compositional implications. Icarus 58, 265–281.

de Pater, I., Dickel, J.R., 1991. Multi-frequency radio observations of Saturn at ring inclination angles between 5 and 26 degrees. Icarus 94, 474–492.

Domingue, D., Verbiscer, A., 1997. Re-analysis of the solar phase curves of the icy Galilean satellites. Icarus 128, 49–74.

Dourneau, G., Baratchart, S., 1999. Masses and densities of the four inner major Saturn's satellites. Astron. Astrophys. 350, 680–684.

Emery, J.P., Burr, D.M., Cruikshank, D.P., Brown, R.H., Dalton, J.B., 2005. Near-infrared (0.8–4.0 μm) spectroscopy of Mimas, Enceladus, Tethys, and Rhea. Astron. Astrophys. 435, 353–362.

Eshleman, V.R., 1986. Radar glory from buried craters on icy moons. Science 234, 587–590.

Evans, J.V., Hagfors, T., 1966. Study of echoes from the Moon at 23 centimeters wavelength. J. Geophys. Res. 71, 4871–4889.

Goldstein, R.M., Green, R.R., 1980. Ganymede: Radar surface characteristics. Science 207, 179–180.

Gurrola, E.M., 1985. Interpretation of radar data from the icy Galilean satellites and Triton. Thesis, Stanford University.

Hagfors, T., Dahlstrom, I., Gold, T., Hamran, S.-E., Hansen, R., 1997. Refraction scattering in the anomalous reflections from icy surfaces. Icarus 130, 313–322.

Haldemann, A.F.C., Muhleman, D.O., 1999. Circular-polarization radar properties of high-altitude ice: Western Kunlun Shan and central Andes. J. Geophys. Res. 104, 24075–24094.

Hapke, B., 1990. Coherent backscatter and the radar characteristics of outer planet satellites. Icarus 88, 407–417.

Heiles, C., Perillat, P., Nolan, M., Lorimer, D., Bhat, R., Ghosh, T., Howell, E., Lewis, M., O'Neil, K., Salter, C., Stanimirovic, S., 2000. Main beam and first sidelobe parameters for Arecibo's receiver systems. Technical Report ATOMS 2000-4. NAIC, Arecibo, PR.

Jezek, K.C., Gogineni, P., Shanableh, M., 1994. Radar measurements of melt zones on the Greenland Ice Sheet. Geophys. Res. Lett. 21, 33–36.

Lewis, J.S., 1972. Low temperature condensation from the solar nebula. Icarus 16, 241–252.

Lorenz, R.D., Shandera, S.E., 2001. Physical properties of ammonia-rich ice: Application to Titan. Geophys. Res. Lett. 28 (2), 215–218.

Magri, C., Ostro, S.J., Rosema, K.D., Thomas, M.L., Mitchell, D.L., Campbell, D.B., Chandler, J.F., Shapiro, I.I., Giorgini, J.D., Yeomans, D.K., 1999. Main belt asteroids: Results of Arecibo and Goldstone radar observations of 37 objects during 1980–1995. Icarus 140, 379–407.

Mosqueira, I., Estrada, P.R., 2003. Formation of the regular satellites of giant planets in an extended gaseous nebula. I. Subnebula model and accretion of satellites. Icarus 163, 198–231.

Nicholson, P.D., French, R.G., Campbell, D.B., Margot, J.-L., Nolan, M.C., Black, G.J., Salo, H.J., 2005. Radar imaging of Saturn's rings. Icarus 177, 32–62.

Ostro, S.J., 1993. Planetary radar astronomy. Rev. Mod. Phys. 65, 1235–1280.

Ostro, S.J., Campbell, D.B., Simpson, R.A., Hudson, R.S., Chandler, J.F., Rosema, K.D., Shapiro, I.I., Standish, E.M., Winkler, R., Yeomans, D.K., 1992. Europa, Ganymede, and Callisto—New radar results from Arecibo and Goldstone. J. Geophys. Res. 97, 18227–18244.

Ostro, S.J., and 19 colleagues, 2006. Cassini Radar observations of Enceladus, Tethys, Dione, Rhea, Iapetus, Hyperion, and Phoebe. Icarus 183, 479–490.

Owen, T.C., 2000. On the origin of Titan's atmosphere. Planet. Space Sci. 48, 747–752.

Peters, K., 1992. The coherent backscatter effect: A vector formulation accounting for polarization and absorption effects and small or large scatterers. Phys. Rev. B 46, 801–812.

Plescia, J.B., Boyce, J.M., 1985. Impact cratering history of the saturnian satellites. J. Geophys. Res. 90, 2029–2037.

Porco, C.C., and 24 colleagues, 2006. Cassini observes the active south pole of Enceladus. Science 311, 1393–1401.

Rignot, E.J., Ostro, S.J., van Zyl, J.J., Jezek, K.C., 1993. Unusual radar echoes from the Greenland ice sheet. Science 261, 1710–1713.

Squyres, S.W., Reynolds, R.T., Cassen, P.M., 1983. The evolution of Enceladus. Icarus 53, 319–331.

Thomas, P.C., Veverka, J., Helfenstein, P., Porco, C., Burns, J., Denk, T., Turtle, E., Jacobson, R.A., the ISS Science Team, 2006. Shapes of the saturnian icy satellites. Lunar Planet. Sci. XXXVII, 1639–1640. Abstract.

Thompson, W.R., Squyres, S.W., 1990. Titan and other icy satellites: Dielectric properties of constituent materials and implications for radar sounding. Icarus 86, 336–354.

Verbiscer, A., French, R., Showalter, M., Helfenstein, P., 2007. Enceladus: Cosmic graffiti artist caught in the act. Science 315, 815.

Wagner, R., Roatsch, T., Giese, B., Wolf, U., Neukum, G., 2006. Geologic mapping of the saturnian satellites based on Cassini ISS images: Objectives, methods, and results. In: European Planetary Science Congress, p. 594.

Waite, J.H., and 13 colleagues, 2006. Cassini Ion and Neutral Mass Spectrometer: Enceladus plume composition and structure. Science 311, 1419–1422.

Zahnle, K., Schenk, P., Levison, H., Dones, L., 2003. Cratering rates in the outer Solar System. Icarus 163, 263–289.